NeuroImage 254 (2022) 119168

Contents lists available at ScienceDirect

NeuroImage

journal homepage: www.elsevier.com/locate/neuroimage

Brain tissue microstructural and free-water composition 13 years after very preterm birth

Claire Kelly[a,b,c,†,*], Thijs Dhollander[c,†], Ian H Harding[d,e], Wasim Khan[d], Richard Beare[c], Jeanie LY Cheong[b,f,g], Lex W Doyle[b,f,g,h], Marc Seal[c,h], Deanne K Thompson[b,c,h], Terrie E Inder[i], Peter J Anderson[a,b]

[a] Turner Institute for Brain and Mental Health, School of Psychological Sciences, Monash University, Melbourne, Australia
[b] Victorian Infant Brain Studies (VIBeS), Clinical Sciences, Murdoch Children's Research Institute, Melbourne, Australia
[c] Developmental Imaging, Clinical Sciences, Murdoch Children's Research Institute, Melbourne, Australia
[d] Department of Neuroscience, Central Clinical School, Monash University, Melbourne, Australia
[e] Monash Biomedical Imaging, Monash University, Melbourne, Australia
[f] The Royal Women's Hospital, Melbourne, Australia
[g] Department of Obstetrics and Gynaecology, The University of Melbourne, Melbourne, Australia
[h] Department of Paediatrics, The University of Melbourne, Melbourne, Australia
[i] Department of Pediatric Newborn Medicine, Brigham and Women's Hospital, Harvard Medical School, Boston, MA, USA

ARTICLE INFO

Keywords:
Preterm
Magnetic resonance imaging
Diffusion-weighted imaging
Microstructure

ABSTRACT

There have been many studies demonstrating children born very preterm exhibit brain white matter microstructural alterations, which have been related to neurodevelopmental difficulties. These prior studies have often been based on diffusion MRI modelling and analysis techniques, which commonly focussed on white matter microstructural properties in children born very preterm. However, there have been relatively fewer studies investigating the free-water content of the white matter, and also the microstructure and free-water content of the cortical grey matter, in children born very preterm. These biophysical properties of the brain change rapidly during fetal and neonatal brain development, and therefore such properties are likely also adversely affected by very preterm birth. In this study, we investigated the relationship of very preterm birth (<30 weeks' gestation) to both white matter *and* cortical grey matter microstructure *and* free-water content in childhood using advanced diffusion MRI analyses. A total of 130 very preterm participants and 45 full-term control participants underwent diffusion MRI at age 13 years. Diffusion tissue signal fractions derived by Single-Shell 3-Tissue Constrained Spherical Deconvolution were used to investigate brain tissue microstructural and free-water composition. The tissue microstructural and free-water composition metrics were analysed using a voxel-based analysis and cortical region-of-interest analysis approach. Very preterm 13-year-olds exhibited reduced white matter microstructural density and increased free-water content across widespread regions of the white matter compared with controls. Additionally, very preterm 13-year-olds exhibited reduced microstructural density and increased free-water content in specific temporal, frontal, occipital and cingulate cortical regions. These brain tissue composition alterations were strongly associated with cerebral white matter abnormalities identified in the neonatal period, and concurrent adverse cognitive and motor outcomes in very preterm children. The findings demonstrate brain microstructural and free-water alterations up to thirteen years from neonatal brain abnormalities in very preterm children that relate to adverse neurodevelopmental outcomes.

1. Introduction

Over 10% of births every year are preterm (<37 weeks' gestational age) (Chawanpaiboon et al., 2019). Preterm birth is associated with increased risk for neonatal brain injury or abnormalities, primarily in the vulnerable immature cerebral white matter (WM), with secondary dysmaturation of cortical and subcortical grey matter (GM) (Volpe, 2019). Research of the consequences of preterm birth on the later developmental dysmaturation that may occur following neonatal brain injury or abnormalities is needed to understand the high rates of adverse neu-

* Corresponding author: Claire Kelly, Turner Institute for Brain and Mental Health, School of Psychological Sciences, 18 Innovation Walk, Monash University, Clayton, VIC, 3800, Australia
E-mail address: claire.kelly@monash.edu (C. Kelly).
† CK and TD contributed equally to this work.

https://doi.org/10.1016/j.neuroimage.2022.119168.
Received 19 November 2021; Received in revised form 27 February 2022; Accepted 30 March 2022
Available online 1 April 2022.

rodevelopmental outcomes reported in preterm children (Saigal and Doyle, 2008).

Key magnetic resonance imaging (MRI) studies have reported altered brain volumes in very preterm (VP; <32 weeks' gestational age) infants, children and adolescents compared with full-term (FT) controls, including in frontal, occipital, temporal, and cingulate cortical GM regions (de Kieviet et al., 2012; Hadaya and Nosarti, 2020; Keunen et al., 2012; Zhou et al., 2018). However, brain volume per se does not reflect the *microstructural* brain properties affected by VP birth. Thus, *diffusion-weighted* MRI data has been analysed using the diffusion tensor imaging (DTI) model, identifying altered microstructure in widespread periventricular and non-periventricular WM regions in VP infants, children and adolescents compared with FT controls (Dibble et al., 2021; Li et al., 2015; Pandit et al., 2013). Despite being commonly used, DTI measures provide limited information on biological mechanisms underlying reported findings, as they are not specific to particular microstructural properties and are confounded by extra-axonal signal and fibre geometry (Jones et al., 2013). Some recent studies applied advanced diffusion MRI models and analysis frameworks such as Neurite Orientation Dispersion and Density Imaging (NODDI) (Kelly et al., 2016; Young et al., 2019) and fixel-based analysis (Kelly et al., 2020; Pannek et al., 2018; Pecheva et al., 2019), showing VP birth is associated more specifically with reduced WM axon density in many WM fibre tracts.

Thus, as described above, prior diffusion MRI studies in VP-born children have commonly focussed on the microstructure of the WM, with relatively fewer studies also investigating other measures such as free-water content in the WM, and in other regions such as the cortical GM, in VP-born children. These biophysical properties of the brain change rapidly during fetal and neonatal brain development (Ouyang et al., 2019), and therefore such properties are likely adversely affected by VP birth. Recent diffusion MRI advancements, such as Single-Shell 3-Tissue Constrained Spherical Deconvolution (SS3T-CSD), enable investigation of brain WM and cortical GM microstructure and free-water properties (Dhollander and Connelly, 2016). SS3T-CSD has been applied to study the microstructural and free-water properties of typically developing brain tissue (Dhollander et al., 2019a), and pathological tissue in neurodegenerative diseases (Khan et al., 2020; Khan et al., 2021; Mito et al., 2020). In these applications, tissue is characterised in terms of its relative composition of "WM-like" (T_W), "GM-like" (T_G), and "CSF-like" (T_C, i.e., free-water) *diffusion signal* characteristics. For example, during typical neonatal brain development, a relative increase in WM-like signal and decrease in CSF-like signal occurs in cerebral WM regions; this temporally corresponds to microstructural axonal and myelin development accompanied by decreasing free-water content in the cerebral WM (Dhollander et al., 2019a). It is important to note that, while these diffusion signal representations are calibrated by the three key diffusion patterns of WM, GM and CSF, they do not imply *biological* similarity. For example, in neurodegenerative diseases, increases in "GM-like" (T_G) signal have been observed in cerebral WM lesions (Khan et al., 2020; Khan et al., 2021; Mito et al., 2020): the relative shift from a "WM-like" (T_W) signal to a more "GM-like" (T_G) signal in these WM lesions is compatible with axon and myelin loss and gliosis, which shares no biological resemblance to GM, yet from a diffusion signal point of view effectively indicates slightly increased diffusivity and decreased anisotropy.

The effect of VP birth on these three-tissue compositions (T_W, T_G and T_C) has not been investigated. Application of three-tissue compositions would complement and expand prior research to provide information on microstructure and free-water content of the WM and cortical GM in VP-born children and adolescents. In the current study, we aimed to investigate effects of VP birth on brain WM and GM microstructural and free-water properties at age 13 years. As the three-tissue compositions have previously been analysed specifically in WM regions (Khan et al., 2020; Khan et al., 2021; Mito et al., 2020), we employed a bespoke approach to analyse the three-tissue compositions across the whole-brain via a voxel-based analysis (VBA). Additionally, given there have been relatively few prior studies of cortical microstructure in VP children and adolescents, we detailed the three-tissue compositions in cortical regions-of-interest (ROIs). We hypothesised that disruption to early brain development by VP birth is associated with widespread reduced microstructural density (i.e., reduced T_W in the WM and reduced T_G in the cortical GM) and increased free-water content (i.e., increased T_C in the same WM and cortical GM regions) later in childhood (at age 13 years). Additionally, we hypothesise these patterns of tissue composition alterations are more pronounced following neonatal brain injury and abnormalities, and are related to adverse neurodevelopmental outcomes in VP children.

2. Methods

2.1. Participant recruitment

Infants born VP (<30 weeks' gestation or <1250 g) were recruited between July 2001 and December 2003 from the Royal Women's Hospital, Melbourne (a total of n=224 VP infants were recruited). Control infants born FT (≥37 weeks' gestation) were also recruited (a total of n=76 FT infants were recruited). Infants with genetic or congenital abnormalities were excluded. All participants were invited to return for assessments, including MRI, at 13 years of age. Brain volumes and WM microstructure (based on fixel-based analysis) for the VP compared with FT participants in this cohort at age 13 years have been previously reported (Kelly et al., 2020; Thompson et al., 2020). The study was approved by the Human Research and Ethics Committees of the Royal Women's Hospital and The Royal Children's Hospital, Melbourne, and parents gave written informed consent.

2.2. Perinatal data collection

Extensive data were collected in the perinatal period and were used in the current study for the purpose of correlating with brain tissue composition data at age 13 years. These perinatal data included the following variables: gestational age at birth; sex; birth weight standardised for gestational age and sex (birth weight z-score) (Cole et al., 1998); major neonatal brain injuries (intraventricular haemorrhage (Papile et al., 1978) and cystic periventricular leukomalacia, which were diagnosed by serial cranial ultrasound prior to term-equivalent age in the VP group); neonatal infection (which was defined as the presence of sepsis and/or proven necrotizing enterocolitis); neonatal brain abnormalities (which were assessed from MRI at term-equivalent age, i.e., 38-42 weeks' postmenstrual age, using an established scoring system (Kidokoro et al., 2013)). The neonatal cranial ultrasound and the neonatal MRI variables were analysed separately.

2.3. 13-year neurodevelopmental assessments

IQ was estimated using the Kaufman Brief Intelligence Test, Second Edition (KBIT2) (Kaufman and Kaufman, 1997), with a mean (M) of 100 and standard deviation (SD) of 15. Motor ability was assessed using the total motor score (M=10, SD=3) from the Movement Assessment Battery for Children, Second Edition (MABC-2) (Henderson et al., 2007).

2.4. 13-year MRI

MRI data were acquired using a 3T Siemens Trio scanner at the Royal Children's Hospital, Melbourne. Diffusion MRI data were acquired with 60 gradient directions, b=2800 s/mm^2, 4 b=0 s/mm^2 images, repetition time= 3200 ms, echo time=110 ms, and 2.4 mm isotropic voxels. T_1-weighted anatomical images were also acquired with 0.9 mm isotropic voxels. Brain volumes were derived from the T_1-weighted images as previously described (Thompson et al., 2020).

2.5. Diffusion MRI pre-processing and modelling

Diffusion MRI image processing was predominantly performed using the MRtrix3 (Tournier et al., 2019), MRtrix3Tissue

(https://3Tissue.github.io, a fork of MRtrix3), and FSL (Jenkinson et al., 2012) software packages. Preprocessing included Gibbs-ringing correction (Kellner et al., 2016), motion and distortion correction (Andersson et al., 2017; Andersson et al., 2016; Andersson and Sotiropoulos, 2016; Schilling et al., 2019), estimation and averaging of 3-tissue response functions (Dhollander et al., 2019b), upsampling to 1.5 mm isotropic voxels, SS3T-CSD (Dhollander and Connelly, 2016), and global intensity normalisation and bias field correction (Dhollander et al., 2021). Diffusion image quality was high as determined by visual inspection and automatically using the FSL QUAD and SQUAD tools (Bastiani et al., 2019). These steps ultimately resulted in the WM (fibre orientation distribution), GM and CSF signal compartment images for each participant. A WM fibre orientation distribution population template for the study was made by iteratively normalising and averaging 30 (15 VP, 15 FT) participants' images using a symmetric diffeomorphic fibre orientation distribution-based image registration algorithm (Raffelt et al., 2011).

2.6. Tissue signal fraction map generation

Each participant's WM, GM and CSF signal compartment images were registered to the template (Raffelt et al., 2011). Registration accuracy for all participants was ensured by visual inspection. After this, each compartment was divided by the sum of all three compartments. This generated the WM-like, GM-like and CSF-like *tissue signal fraction maps*, denoted as T_W, T_G and T_C respectively (Khan et al., 2020; Khan et al., 2021; Mito et al., 2020). These tissue signal fractions have previously been described extensively (Khan et al., 2020; Khan et al., 2021; Mito et al., 2020). The reliability and long-term stability of these tissue signal fractions has also been established previously (Newman et al., 2020).

2.7. Whole-brain VBA

The tissue signal fraction maps were smoothed (full width half maximum=4mm) and analysed via voxel-based analysis (VBA) with general linear modelling, threshold-free cluster enhancement and non-parametric permutation testing (Smith and Nichols, 2009). Statistical analyses were restricted to brain parenchyma (i.e., excluding the ventricles). The tissue signal fractions were compared between the VP and FT groups, and correlated with each perinatal risk factor and neurodevelopmental outcome separately in the VP group only, adjusted for age and sex. This primary analysis correlated the tissue signal fractions with IQ and motor scores in the VP group only, because we were interested in investigating whether tissue composition alterations correlated with the higher rates of adverse IQ and motor outcomes that have been reported in VP children (Saigal and Doyle, 2008). We then also performed secondary analyses to correlate the tissue signal fractions with cognitive and motor outcomes in all participants (VP and FT), and investigate whether relationships of the tissue signal fractions with cognitive and motor outcomes differed *between* the VP and FT participants (i.e., a group-by-outcome interaction analysis). Statistical significance was defined as $p<0.05$, after correction for the family-wise error rate.

2.8. Cortical ROI analysis

Given the challenges and limitations with aligning cortical regions to a template in the VBA, which could potentially mean the VBA does not provide a clear representation of group differences or correlations with clinical factors in cortical regions, we performed an additional cortical ROI analysis in native (subject) space. The T_1-weighted images were aligned to the diffusion MRI data and processed using FreeSurfer (Fischl, 2012). Region-averaged T_W, T_G and T_C values were sampled from 34 cortical regions per hemisphere defined using the Desikan-Killiany atlas (Fig. 1) (Desikan et al., 2006). These data were then analysed using a previously described framework for 3-tissue compositional data analysis (Dhollander et al., 2019a). This analysis involved transforming the average T_W, T_G and T_C values for each cortical region into a pair of isometric log-ratios (ilr_1 and ilr_2). This *ilr* transform is designed to account for the interdependence and boundedness of the 3 signal fractions (i.e., $T_W + T_G + T_C = 1$ and all are bounded between 0 and 1), allowing for multivariate analyses (e.g., MANCOVAs) (Khan et al., 2020; Khan et al., 2021; Mito et al., 2020). The *ilr* transformed values were compared between the VP and FT groups, and correlated with each perinatal risk factor and neurodevelopmental outcome separately in the VP group, adjusted for age and sex, using R version 3.6.3. From each of these analyses, we obtained a (single) false discovery rate-corrected *p*-value for each test in each cortical region, indicating whether the 3-tissue composition "as a whole" significantly differed between the groups, or was significantly correlated with the clinical variables in that region. These *p*-values were visualised on the semi-inflated white matter surface using ggseg3d (Mowinckel and Vidal-Piñeiro, 2019). The *ilr* values can thus be used for indicating whether there is a significant difference in, or correlation with, the overall tissue composition; however, further *interpretation* of any effects relies on the original T_W, T_G and T_C values themselves, which can be visualised using ternary plots for this purpose.

3. Results

3.1. Participant characteristics

Of the 224 VP infants and 76 FT infants recruited, a total of 179 VP children and 61 FT children were followed up at age 13 years, of which 141 VP children and 47 FT children underwent MRI. The main reasons that participants were not followed up at age 13 years included families declining or withdrawing from the study, living in other countries, or being unable to be contacted (Thompson et al., 2020). Of the participants who underwent MRI at age 13 years, 130 VP participants and 45 FT participants had images suitable for analysis in the current study. Exclusions were due to incomplete or incorrect image acquisitions (n=11) or movement-induced artefacts (n=2). Age at MRI and sex did not differ significantly between the VP and FT groups (Table 1). The VP group had more brain MRI abnormalities in the neonatal period, and lower intracranial volume, total WM volume, total cortical GM volume, IQ and motor scores at age 13 years compared with the FT group (Table 1). Baseline perinatal characteristics did not differ significantly between participants compared with non-participants (who were recruited but not included in the current study; all $p>0.05$). Relationships between perinatal and neurodevelopmental variables within the VP group are provided in Supplementary Table S1 which is within Supplementary Document 2.

3.2. Results of the whole-brain VBA

Compared with the FT group, the VP group exhibited significantly (family-wise error corrected $p<0.05$) lower "WM-like" diffusion signal (T_W), higher "GM-like" signal (T_G), and higher "CSF-like" signal (T_C) in substantial parts of the WM, including the corpus callosum, cingulum, superior and inferior longitudinal fasciculus, tapetum, uncinate fasciculus, anterior and posterior limb of the internal capsule, external capsule, optic radiation, fornix/stria terminalis, anterior commissure, and cerebellar white matter (p-values are shown in Fig. 2; effect sizes are shown in Supplementary Fig. S1 which is within Supplementary Document 2). To demonstrate this relative shift from a WM-like signal towards a more GM-like and/or CSF-like signal in WM regions, we additionally delineated specific periventricular and non-periventricular WM regions in template space (Wasserthal et al., 2018), and extracted and plotted tissue compositions in these regions (Supplementary Fig. S2 within Supplementary Document 2).

Concurrently, in portions of the *cortical GM* we observed significantly lower T_G and higher T_C in the VP group compared with

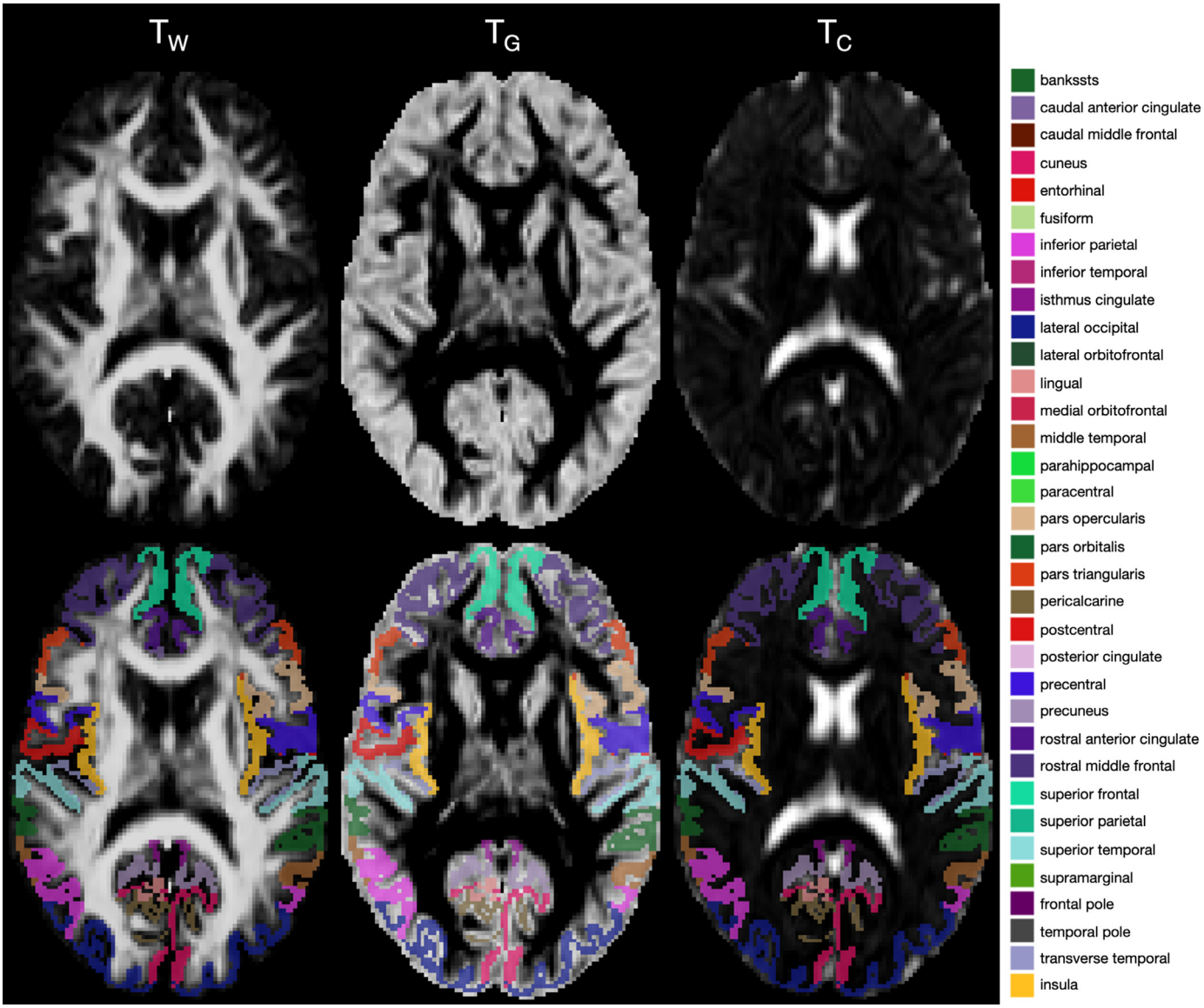

Fig. 1. T_W, T_G and T_C maps for a randomly chosen representative participant, without (top row) and with (bottom row) the cortical regions of interest overlaid.

Table 1
Characteristics of the very preterm (VP) and full-term (FT) participants.

Characteristic	VP, *n*=130	FT, *n*=45	*p*
Perinatal characteristics			
Gestational age at birth (weeks), M (SD)	27.4 (1.9)	39.0 (1.4)	NA
Birth weight (g), M (SD)	966 (231)	3316 (552)	NA
Birth weight (z-score), M (SD)	-0.5 (1.0)	0.1 (0.9)[a]	NA
Males, *n* (%)	70 (54)	22 (49)	0.6
Intraventricular haemorrhage grade 3/4 from cranial ultrasound, *n* (%)	7 (5)	NA	NA
Cystic periventricular leukomalacia from cranial ultrasound, *n* (%)	4 (3)	NA	NA
Neonatal infection, *n* (%)	41 (32)	0 (0)[a]	0.001
Moderate-severe neonatal global brain MRI abnormality score, *n* (%)	28 (24)[b]	0 (0)[c]	0.009
Neonatal global brain MRI abnormality score, M (SD)	5.3 (3.1)[b]	1.6 (1.4)[c]	<0.001
13-year characteristics			
Age at MRI (years), M (SD)	13.3 (0.4)	13.3 (0.5)	0.98
Intracranial volume (cm^3), M (SD)	1441 (131)	1526 (157)	0.0005
Total white matter volume (cm^3), M (SD)	388 (48)	423 (52)	<0.001
Total cortical grey matter volume (cm^3), M (SD)	566 (55)	595 (65)	0.003
IQ, M (SD)	99.5 (18.0)	109.8 (12.4)	<0.001
Motor performance score, M (SD)	8.5 (3.2)[d]	10.0 (2.2)[e]	0.004

[a] *n*=24. [b]*n*=119. [c]*n*=23. [d]*n*=127. [e]*n*=42. Age at MRI was corrected for prematurity in the VP group.

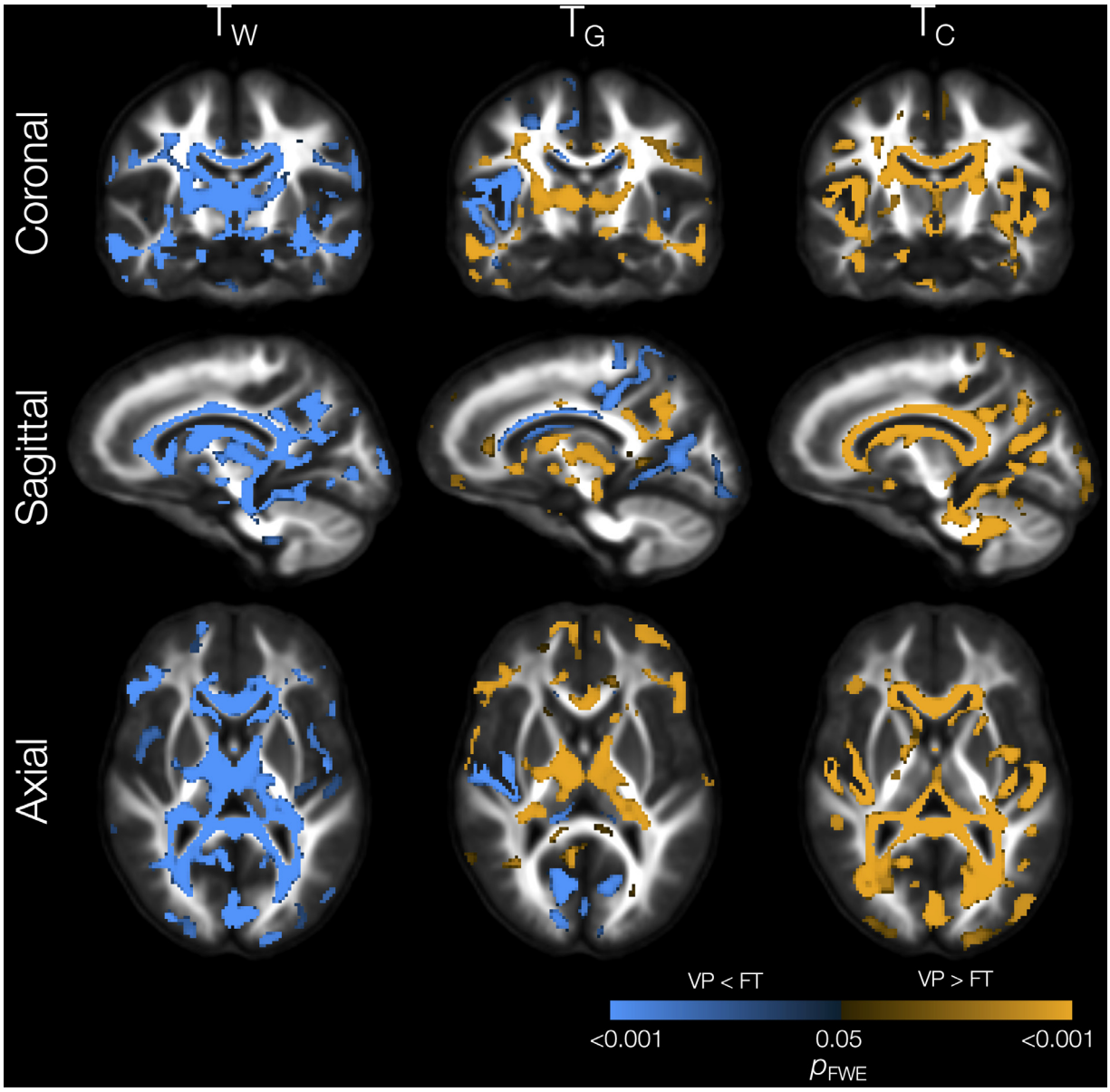

Fig. 2. Results of the whole-brain VBA: significant differences in T_W, T_G and T_C between the VP and FT groups. Widespread decreases in T_W in the WM are accompanied by increases in T_G and/or T_C in similar areas. There are also some cortical decreases in T_G, which are accompanied by increases in T_C. Images are shown in radiological convention (left hemisphere of the brain is shown on the right side of the image).

the FT group. These regions included temporal (superior temporal, transverse temporal), sensorimotor (precentral, paracentral), occipital (pericalcarine, lingual, lateral occipital), cingulate and insula regions (Fig. 2).

These group differences remained similar after excluding the small number of VP children who had major neonatal cystic or haemorrhagic brain injuries on cranial ultrasound (*not shown*).

Lower gestational age at birth and lower birth weight z-score were significantly associated with lower T_W and higher T_G in some small WM regions, including the external capsule, sagittal stratum and corpus callosum (for gestational age; Supplementary Fig. S3 within Supplementary Document 2), and the cingulum, internal capsule, cerebellar white matter, corpus callosum and superior longitudinal fasciculus (for birth weight z-score; Supplementary Fig. S4 within Supplementary Document 2). We found no significant associations between postnatal infection and tissue compositions. Higher neonatal global brain MRI abnormality scores were significantly associated with widespread reductions in T_W and increases in T_G and T_C in the WM, along with some increases in T_C in the cortical GM (Fig. 3). Post-hoc analyses of the neonatal global brain MRI abnormality score subcomponents demonstrated that the WM abnormality score (including measures of focal signal abnormality and dilated lateral ventricles) largely mirrored the global brain abnormality score (i.e., higher neonatal WM abnormality scores were significantly related to reductions in T_W and increases in T_G and T_C in the WM, along with some increases in T_C in the cortical GM). Additionally, higher neonatal *cortical GM* abnormality scores were significantly related to lower T_G in some medial frontal, parietal and cingulate cortical GM regions. Furthermore, post-hoc analyses showed that higher neonatal global brain MRI abnormality scores were related to lower global brain WM and cortical GM volumes at 13 years of age in the same participants (all $p<0.05$), which highlights that neonatal brain abnormalities have effects at age 13 years that are visible with complementary MRI techniques, including volumetric, microstructural and free-water alterations of the WM and cortical GM.

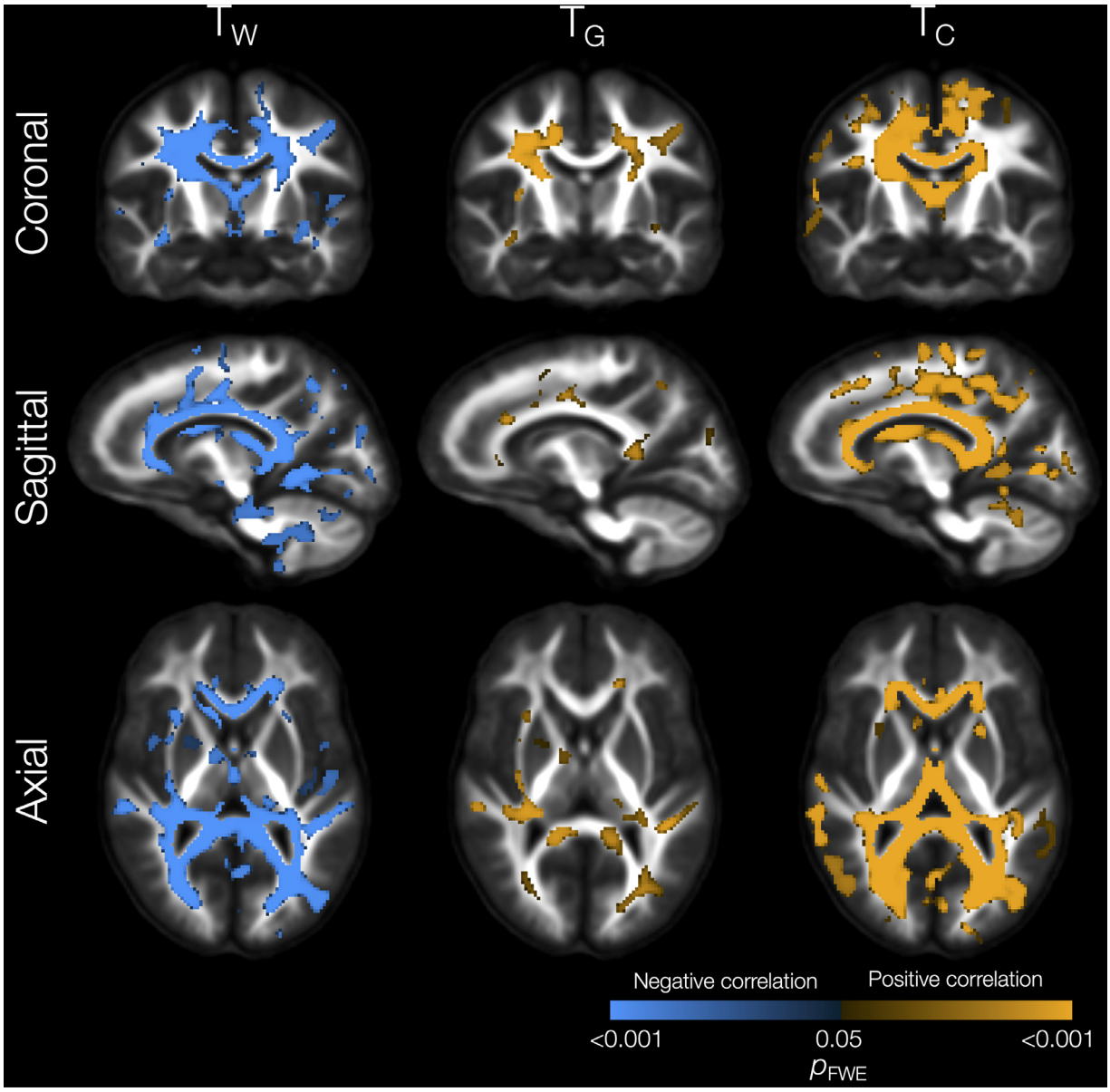

Fig. 3. Results of the whole-brain VBA: significant correlations of neonatal brain abnormality score with T_W, T_G and T_C in the VP group. Widespread negative correlations between neonatal brain abnormality and T_W in the WM are accompanied by positive correlations with T_G and/or T_C in similar areas. T_C also showed positive correlations in some cortical areas. Images are shown in radiological convention (left hemisphere of the brain is shown on the right side of the image).

Lower T_W and higher T_G and T_C in several WM regions, including the corpus callosum, internal and external capsules, superior and inferior longitudinal fasciculus, cingulum, and cerebellar white matter, were significantly associated with lower IQ scores at age 13 years in the VP group (Fig. 4). Lower T_W, higher T_G and higher T_C throughout the WM, and higher T_C throughout the cortical GM, were significantly associated with poorer motor scores at age 13 years in the VP group (Fig. 5). In secondary analyses when including all participants (VP and FT), we found that 1. relationships of tissue compositions with IQ scores were similar but more spatially dispersed, while relationships with motor scores were similar (Supplementary Fig. S5 and S6 within Supplementary Document 2); 2. relationships between tissue compositions and IQ and motor scores did not differ significantly *between* the VP and FT groups (all group-by-outcome interaction $p_{FWE} \geq 0.05$), suggesting the relationships hold for both VP and typically developing children.

3.3. Results of the cortical ROI analysis

Several cortical regions were identified in which the overall 3-tissue composition differed significantly (false discovery rate-corrected $p<0.05$) between the groups (Fig. 6). These cortical regions were located across the cortical GM in similar regions as those obtained from the VBA, including the following regions: temporal (superior temporal, banks superior temporal, transverse temporal), occipital (lateral occipital, pericalcarine, lingual), frontal (precentral, paracentral, caudal middle frontal), parietal (inferior parietal), cingulate (isthmus cingulate, rostral anterior cingulate) and insula (Fig. 6). These regions generally exhibited a relative shift from a GM-like signal (T_G) towards a more fluid-like signal (T_C) in the VP group compared with the FT group, as is demonstrated in the ternary plot for one representative significant (false discovery rate-corrected $p<0.05$) temporal region in Fig. 7. Ternary plots showing the relative WM-like, GM-like and CSF-like signal fractions for

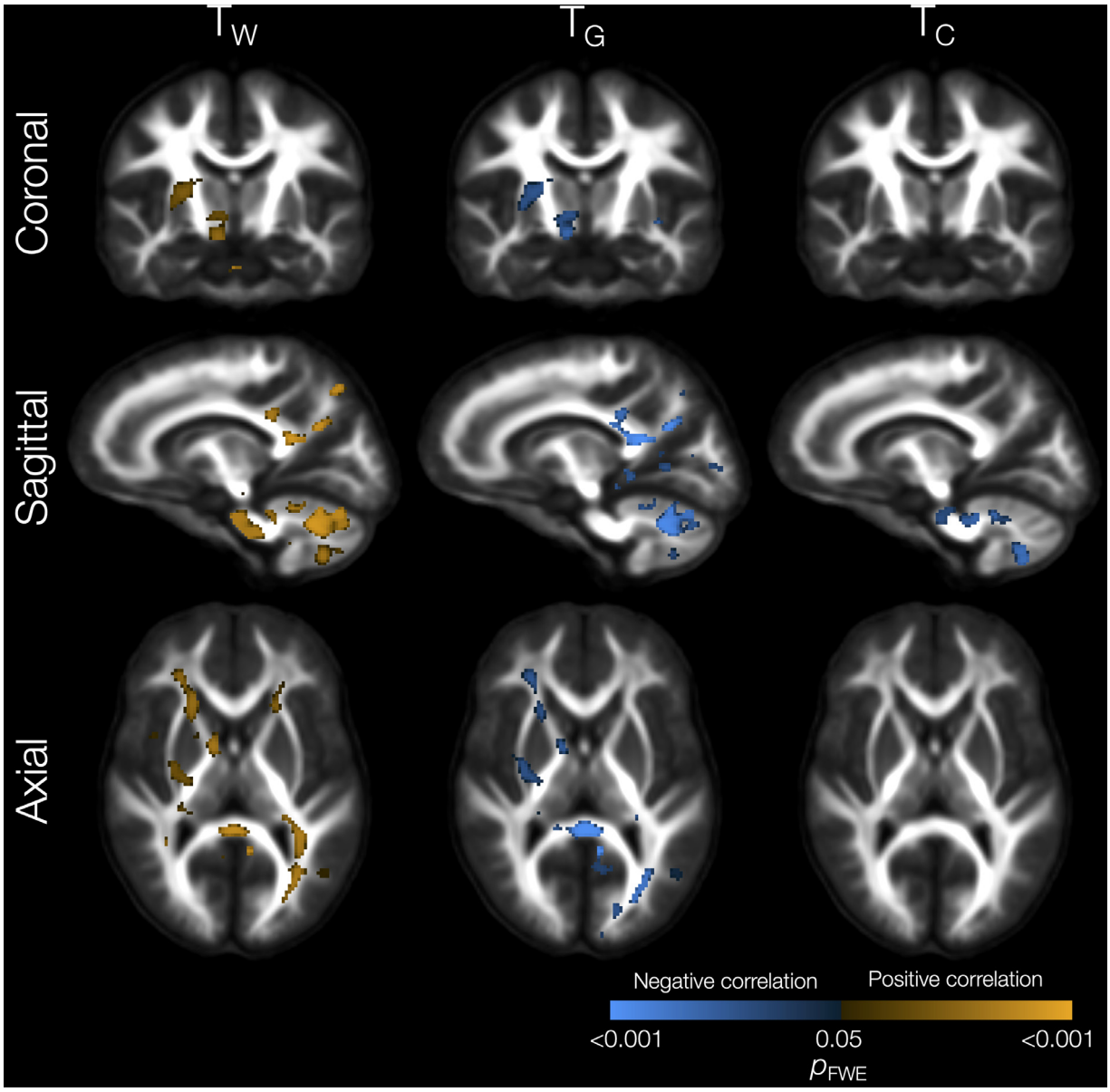

Fig. 4. Results of the whole-brain VBA: significant correlations of T_W, T_G and T_C with IQ scores in the VP group. Small specific areas in the WM show positive correlations between IQ and T_W, most of which are accompanied by negative correlations with T_G and some with T_C. Images are shown in radiological convention (left hemisphere of the brain is shown on the right side of the image).

all the other significant cortical regions are shown in Supplementary Document 1.

No significant associations were identified between gestational age or birth weight and the overall tissue composition in the cortical ROIs, which is in line with the VBA results (in which small, specific associations in the WM but not cortical GM were found). No significant associations were identified between postnatal infection and tissue compositions in cortical regions. However, higher neonatal brain MRI abnormality scores were significantly associated with altered tissue compositions in some cortical regions, located similarly to the VBA, including in the cingulate, parietal (precuneus, superior parietal) and occipital (pericalcarine) cortex (Fig. 6). In general, these cortical regions showed a relative shift towards T_C in association with more severe neonatal brain MRI abnormality scores (as demonstrated in the ternary plot for one representative significant region in Fig. 7; ternary plots for all regions significantly related to neonatal brain abnormality scores are shown in Supplementary Document 1).

Finally, no significant associations between tissue compositions in cortical ROIs and IQ score were identified, in line with the VBA which identified associations with IQ in the WM only. However, several frontal, parietal, occipital, temporal and cingulate cortical regions were identified in which the overall tissue composition was significantly related to motor scores, analogous to the VBA results (Fig. 6). In general, these cortical regions demonstrated a relative shift towards T_C in relation to poorer motor scores (as demonstrated in the ternary plot for one representative significant region in Fig. 7; ternary plots for all regions significantly related to motor scores are shown in Supplementary Document 1).

4. Discussion

We found that VP adolescents exhibited microstructural alterations and increased free-water content across substantial parts of the brain parenchyma compared with FT controls. In the WM, microstructural

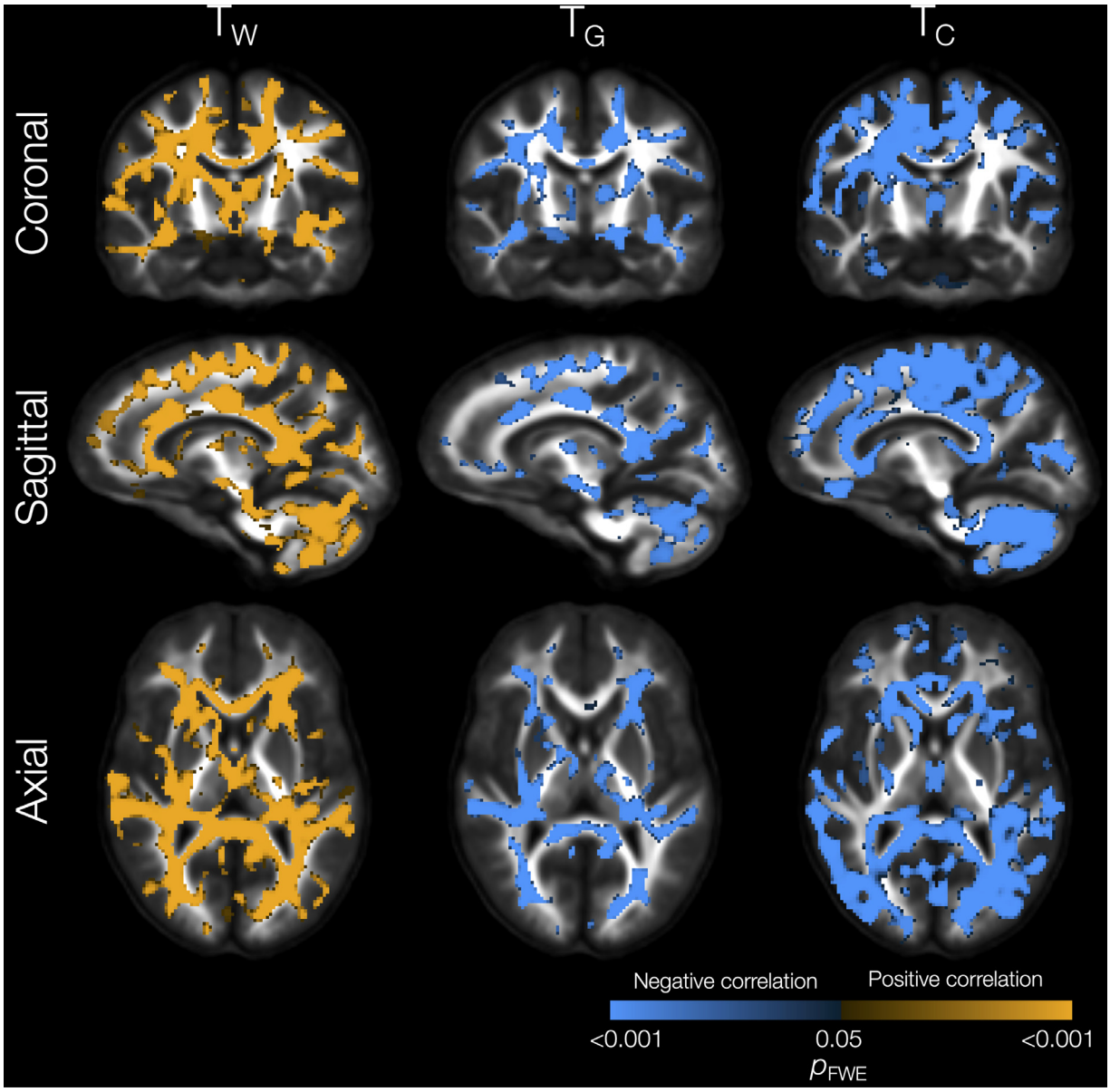

Fig. 5. Results of the whole-brain VBA: significant correlations of T_W, T_G and T_C with motor scores in the VP group. Widespread positive correlations between motor scores and T_W in the WM are accompanied by negative correlations with T_G and/or T_C in similar areas. T_C also showed negative correlations in several cortical areas. Images are shown in radiological convention (left hemisphere of the brain is shown on the right side of the image).

alterations were widespread and occurred as a relative shift from the expected "WM-like" (T_W) composition towards a more "GM-like" (T_G) or fluid-like (T_C) composition. These WM microstructural alterations occurred alongside microstructural alterations in several portions of the cortical GM, where VP adolescents generally exhibited a relative shift from a "GM-like" (T_G) composition towards a more fluid-like (T_C) composition, based on converging evidence from both a whole-brain and region-specific analysis. The tissue composition alterations were particularly pronounced in VP 13-year-olds who had neonatal brain abnormalities. Tissue composition alterations were also related to adverse neurodevelopmental outcomes in both VP and FT children, demonstrating a) widespread regions related to motor outcomes, and b) relatively more specific regions related to cognitive outcomes.

In the WM, the relative shift from a WM-like composition towards a more GM-like or fluid-like composition in the VP 13-year-olds compared with controls may reflect reduced axon density or reduced myelination that is compensated for by increased extra-axonal fluid, cells or macromolecules. Note that the GM-like signal (T_G) in this context does not imply *biological, functional or chemical* similarity to GM, but reflects similar *diffusion signal characteristics* (Khan et al., 2020; Khan et al., 2021; Mito et al., 2020). The tissue composition alterations were located in widespread WM regions, particularly in periventricular WM regions which are common sites of perinatal WM injury in VP infants (Volpe, 2019), affecting WM tracts such as the corpus callosum, tapetum, corticospinal tract, optic radiation and inferior longitudinal fasciculus. The tissue composition alterations were also located diffusely in non-periventricular WM regions such as the cingulum, uncinate fasciculus and superior longitudinal fasciculus. Several previous studies, including studies based on the current cohort, have reported that VP birth is associated with reduced global WM volumes (de Kieviet et al., 2012; Thompson et al., 2020) and widespread WM microstructural alterations based on alternative diffusion MRI analysis techniques (Dibble et al., 2021; Kelly et al., 2016; Kelly et al., 2020; Li et al., 2015; Pandit et al., 2013; Pannek et al., 2018; Young et al., 2019). Compared with prior

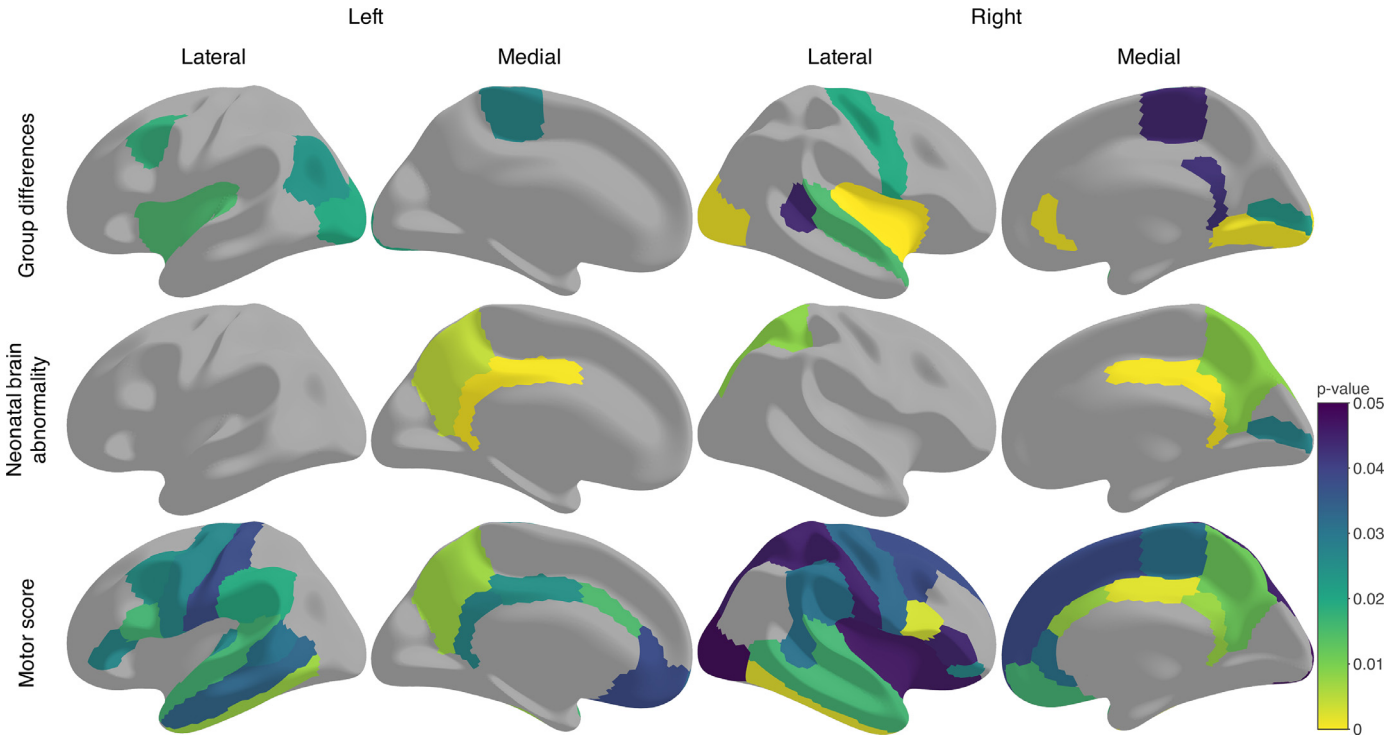

Fig. 6. Results of the cortical ROI analysis: cortical regions in which the overall 3-tissue composition differed significantly between the VP and FT groups (*top row*), was significantly associated with neonatal brain abnormality scores (*middle row*) and was significantly associated with motor scores (*bottom row*). These results were obtained by performing a "compositional data analysis", involving converting the original 3-tissue compositions (T_W, T_G and T_C) to an unbounded 2D space via an isometric log ratio (*ilr*) transform, after which multivariate statistical analysis of the *ilr* transformed values could be performed, in order to investigate the overall tissue composition. For interpretation of the direction of the overall significant group differences in, or significant associations with, the 3-tissue composition, the plots of the original T_W, T_G and T_C values in Fig. 7 and Supplementary Document 1 should be referred to.

studies, the current study provides novel neurobiological insights, by demonstrating that VP birth is associated with reduced microstructural density which is accompanied by increases in extra-axonal free-water content or other cells throughout the WM.

For the cortical GM, the relative shift from a GM-like composition towards a more fluid-like composition in the VP adolescents compared with controls reflects an increase in diffusivity in these regions, from a diffusion signal representation perspective. From a biological perspective, this may reflect decreased GM cell density and increased free-water content in these regions. Microstructural alterations were found in several regions across the cortex including temporal, frontal, parietal, occipital and cingulate regions, with particularly significant alterations in temporal regions, which have established vulnerability in VP children and adolescents based on volumetric and morphological (e.g., cortical folding) measures derived from structural MRI data (Nosarti et al., 2008; Thompson et al., 2020; Zhang et al., 2015). Our findings are also broadly in line with previous studies reporting increased mean diffusivity as derived from DTI in the cortex of preterm-born infants compared with term-born controls, including in frontal, occipital, temporal and parietal regions (Ball et al., 2013; Bouyssi-Kobar et al., 2018; Smyser et al., 2016). To date, there has been little research on cortical microstructure beyond the neonatal period into childhood and adolescence following VP birth. Furthermore, group differences in the cortical GM were similar in both our whole-brain VBA and cortical ROI analysis, supporting the concordance of the measures.

Tissue composition alterations in distributed WM regions, along with some cortical GM regions, were associated with neonatal brain abnormality. These regions resembled the regions that differed between the VP and FT groups, suggesting that neonatal brain injury and abnormality contributed to the observed group differences. The regions also included regions known to be commonly affected by perinatal brain injury in VP infants, particularly posterior periventricular regions (Volpe, 2019). Overall, this provides evidence that the tissue composition alterations at age 13 years reflect long-term consequences of neonatal brain injury or dysmaturation. Prior studies, including studies based on the current cohort, have reported that neonatal brain injury including neonatal white matter injury is associated with altered brain volumes and microstructure in VP infants, children and adolescents (Kelly et al., 2020; Keunen et al., 2012; Smyser et al., 2016; Thompson et al., 2020; Young et al., 2019). Taken together, prior studies and the current study highlight that neonatal brain injury and abnormality is associated with diverse brain volumetric and microstructural alterations of the WM and GM in those born VP, with the current study establishing specifically that neonatal brain abnormalities are related to both altered WM and cortical GM microstructural and free-water composition. Lower gestational age and birth weight z-score were also associated with tissue composition alterations, although these associations were comparatively weaker and confined to small, specific WM regions. Tissue compositions across the WM, and sometimes in the cortical GM, were in turn related to cognitive and motor scores, suggesting they play an important role in cognitive and motor development, and that alterations to tissue compositions are likely to contribute to the disproportionately high rates of cognitive and motor impairments reported in the VP population. Somewhat surprisingly, postnatal infection was not related to tissue compositions. Future studies employing measures from the fetal period (for example, chorioamnionitis) may provide more information on the effects of early infection and inflammation on brain microstructural development (Anblagan et al., 2016).

To understand the neurobiological mechanisms potentially underlying our findings, observations from histological studies can be drawn on. These studies suggest that inflammatory and hypoxic-ischaemic insults during the preterm period impair pre-oligodendrocyte maturation

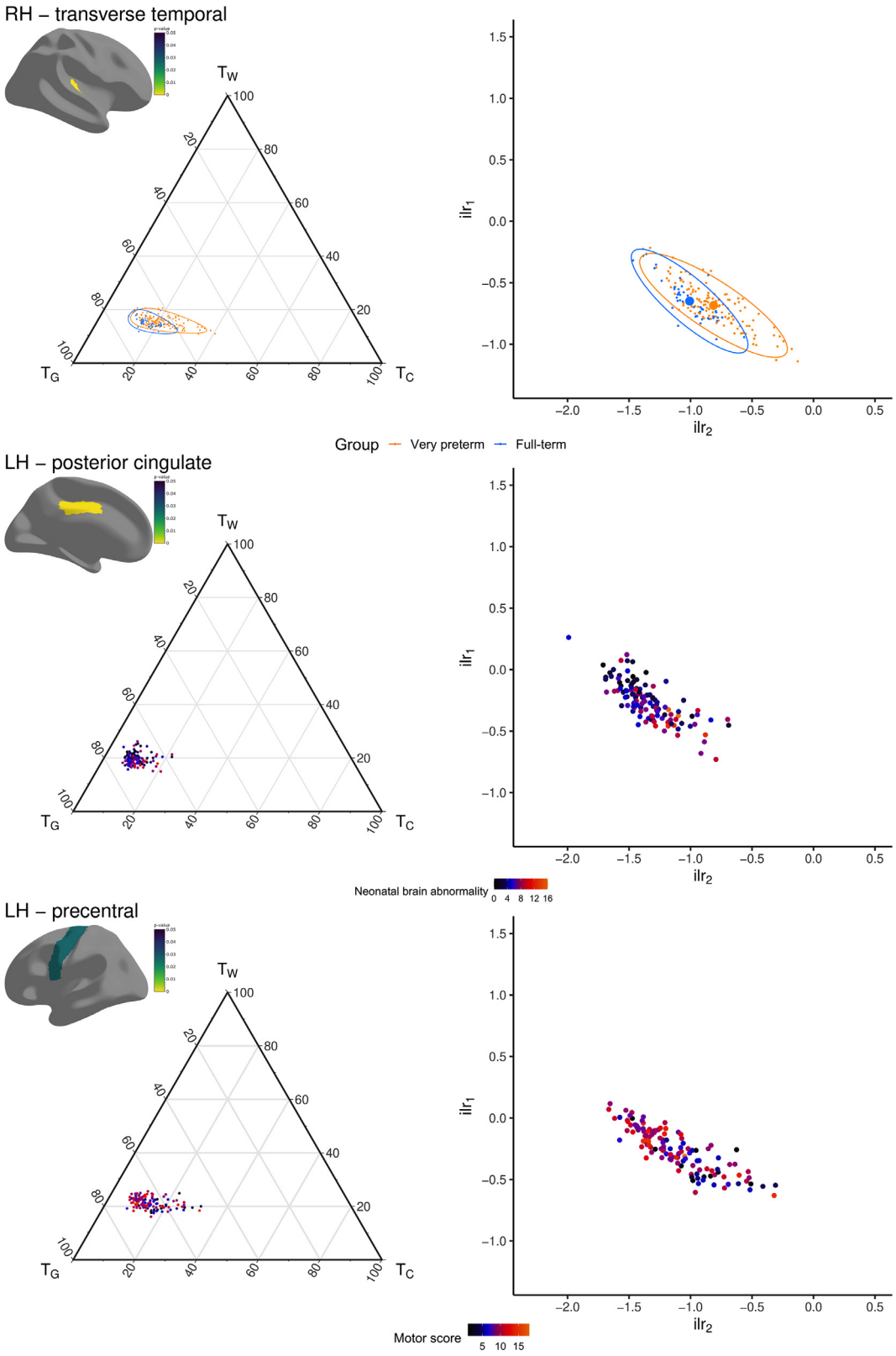

Fig. 7. Results of the cortical ROI analysis. For an example cortical region in which the overall tissue composition significantly differed between groups (*top row*), was significantly correlated with neonatal brain abnormality score (*middle row*), or was significantly correlated with motor score (*bottom row*), this figure shows: a ternary plot of the relative tissue signal fractions of WM-like (T_W), GM-like (T_G), and CSF-like (T_C) signal (as a percentage) per participant (*left column*) and a scatter plot of the isometric log-ratio (*ilr*) transformed equivalent of the tissue compositions (*right column*). The scatter plots indicate the overall significant group difference in tissue composition (*top row, right column*), or the overall significant correlation between neonatal brain abnormality or motor score and tissue composition (*middle and bottom rows, right column*). The ternary plots highlight the relative shift from a GM-like composition (T_G) towards a more fluid-like composition (T_C) in the very preterm group (*top row, left column*) and in relation to increasing neonatal brain abnormality (*middle row, left column*) and decreasing motor score (*bottom row, left column*).

and induce extracellular matrix remodelling and gliosis, which in turn impair subsequent myelination and axonal and cortical development (Volpe, 2019). Our recovered patterns of tissue composition alterations are compatible with the above mechanisms; i.e., they may reflect long-term adverse effects of early neuroinflammatory and hypoxic-ischaemic insults and injury associated with VP birth on the brain WM and GM composition, where reduced WM and GM microstructural density may be accompanied by increased tissue free-water content. The duration of neuroinflammation following VP birth is unknown. Some previous studies have found that gliosis persists chronically into adulthood in mouse models of preterm inflammatory brain injury, occurring with neuron and volume reductions and changes to synaptic function (Kelley et al., 2017).

Whilst our study provides a wealth of novel, specific information on the whole-brain WM and GM microstructural and fluid composition in VP children, relating the results to the real underlying biophysical and biological mechanisms remains challenging. Additional research correlating the tissue compositions with histological data would be useful to provide more direct information on the mechanisms underpinning our findings. Additionally, future multivariate, multimodal studies to directly assess the relationships between various structural and diffusion MRI measures of the WM and GM may shed further light on the mechanisms underlying brain injury and altered brain maturation following VP birth. Use of myelin imaging techniques (Lee et al., 2021) may provide further specificity on whether the findings observed in the current study in the WM relate to axon density, myelination or a combination of both. Prior studies have shown VP children exhibit larger ventricular volumes (Thompson et al., 2020), and while we observed microstructural alterations in periventricular regions in the current manuscript, microstructural alterations were also observed diffusely in non-periventricular regions, meaning our results are unlikely to be entirely driven by ventricular volume changes. Additionally, the periventricular WM is a common neuroanatomical site of brain injury in VP infants (Volpe, 2019), which is likely to also be a contributing factor to the strong microstructural alterations we observed in periventricular WM regions.

5. Conclusions

We demonstrated that VP birth is associated with diverse microstructural and free-water alterations across the brain tissue up to 13 years later, which are associated with neonatal brain abnormalities and adverse cognitive and motor outcomes. Ultimately, these findings are hoped to provide a basis for future investigations into stratifying and predicting high-risk VP individuals, and open up avenues for developing and monitoring the efficacy of interventions to improve neurodevelopmental outcomes (for example, pharmacologic agents or modifications to nutritional or environmental factors). Ongoing studies would be beneficial to determine whether tissue composition alterations reduce, persist, or worsen over time with potential implications for life-long health and development in those born VP.

Data and Code Availability Statement

Data and code are available from the corresponding author on reasonable request. Data are not publicly available due to ethical restrictions.

Conflicts of Interest

Nothing to report.

Credit authorship contribution statement

Claire Kelly: Conceptualization, Formal analysis, Investigation, Visualization, Writing – original draft. **Thijs Dhollander:** Conceptualization, Formal analysis, Investigation, Methodology, Supervision, Visualization, Writing – original draft. **Ian H Harding:** Conceptualization, Writing – review & editing. **Wasim Khan:** Formal analysis, Writing – review & editing. **Richard Beare:** Formal analysis, Writing – review & editing. **Jeanie LY Cheong:** Conceptualization, Funding acquisition, Resources, Supervision, Writing – review & editing. **Lex W Doyle:** Conceptualization, Funding acquisition, Resources, Supervision, Writing – review & editing. **Marc Seal:** Conceptualization, Funding acquisition, Resources, Supervision, Writing – review & editing. **Deanne K Thompson:** Conceptualization, Funding acquisition, Resources, Supervision, Writing – review & editing. **Terrie E Inder:** Conceptualization, Funding acquisition, Resources, Supervision, Writing – review & editing. **Peter J Anderson:** Conceptualization, Funding acquisition, Resources, Supervision, Writing – review & editing.

Acknowledgments

We thank members of the VIBeS and Developmental Imaging teams at the Murdoch Children's Research Institute, the Royal Children's Hospital Medical Imaging staff for their assistance and expertise in the collection of the MRI data included in this study, and the children and families who participated. This research was supported by the Australian National Health and Medical Research Council [NHMRC; Project Grants 237117, 491209 and 1066555; Centre of Clinical Research Excellence 546519; Centre of Research Excellence 1060733 and 1153176; Investigator Grant 1176077 to PA; Career Development Fellowship 1085754 to DT and 1141354 to JC], an Australian Government Research Training Program (RTP) Scholarship and Monash Graduate Excellence Scholarship (CK), the Murdoch Children's Research Institute, the Royal Children's Hospital, the Royal Children's Hospital Foundation, the Department of Paediatrics at the University of Melbourne, and the Victorian Government's Operational Infrastructure Support Program. The funding sources had no role in study design; in the collection, analysis and interpretation of data; in the writing of the report; and in the decision to submit the article for publication.

Supplementary materials

Supplementary material associated with this article can be found, in the online version, at doi:10.1016/j.neuroimage.2022.119168.

References

Anblagan, D., Pataky, R., Evans, M.J., Telford, E.J., Serag, A., Sparrow, S., Piyasena, C., Semple, S.I., Wilkinson, A.G., Bastin, M.E., Boardman, J.P., 2016. Association between preterm brain injury and exposure to chorioamnionitis during fetal life. Sci. Rep. 6, 37932. doi:10.1038/srep37932.

Andersson, J.L.R., Graham, M.S., Drobnjak, I., Zhang, H., Filippini, N., Bastiani, M., 2017. Towards a comprehensive framework for movement and distortion correction of diffusion MR images: Within volume movement. Neuroimage 152, 450–466. doi:10.1016/j.neuroimage.2017.02.085.

Andersson, J.L.R., Graham, M.S., Zsoldos, E., Sotiropoulos, S.N., 2016. Incorporating outlier detection and replacement into a non-parametric framework for movement and distortion correction of diffusion MR images. Neuroimage 141, 556–572. doi:10.1016/j.neuroimage.2016.06.058.

Andersson, J.L.R., Sotiropoulos, S.N., 2016. An integrated approach to correction for off-resonance effects and subject movement in diffusion MR imaging. Neuroimage 125, 1063–1078. doi:10.1016/j.neuroimage.2015.10.019.

Ball, G., Srinivasan, L., Aljabar, P., Counsell, S.J., Durighel, G., Hajnal, J.V., Rutherford, M.A., Edwards, A.D., 2013. Development of cortical microstructure in the preterm human brain. Proc. Natl. Acad. Sci. U. S. A. 110, 9541–9546. doi:10.1073/pnas.1301652110.

Bastiani, M., Cottaar, M., Fitzgibbon, S.P., Suri, S., Alfaro-Almagro, F., Sotiropoulos, S.N., Jbabdi, S., Andersson, J.L.R., 2019. Automated quality control for within and between studies diffusion MRI data using a non-parametric framework for movement and distortion correction. Neuroimage 184, 801–812. doi:10.1016/j.neuroimage.2018.09.073.

Bouyssi-Kobar, M., Brossard-Racine, M., Jacobs, M., Murnick, J., Chang, T., Limperopoulos, C., 2018. Regional microstructural organization of the cerebral cortex is affected by preterm birth. Neuroimage Clin. 18, 871–880. doi:10.1016/j.nicl.2018.03.020.

Chawanpaiboon, S., Vogel, J.P., Moller, A.B., Lumbiganon, P., Petzold, M., Hogan, D., Landoulsi, S., Jampathong, N., Kongwattanakul, K., Laopaiboon, M., Lewis, C., Rattanakanokchai, S., Teng, D.N., Thinkhamrop, J., Watananirun, K., Zhang, J., Zhou, W., Gulmezoglu, A.M., 2019. Global, regional, and national estimates of levels of preterm birth in 2014: a systematic review and modelling analysis. Lancet Glob. Health 7, e37–e46. doi:10.1016/S2214-109X(18)30451-0.

Cole, T.J., Freeman, J.V., Preece, M.A., 1998. British 1990 growth reference centiles for weight, height, body mass index and head circumference fitted by maximum penalized likelihood. Stat. Med. 17, 407–429 doi:.

de Kieviet, J.F., Zoetebier, L., van Elburg, R.M., Vermeulen, R.J., Oosterlaan, J., 2012. Brain development of very preterm and very low-birthweight children in childhood and adolescence: a meta-analysis. Dev. Med. Child Neurol. 54, 313–323. doi:10.1111/j.1469-8749.2011.04216.x.

Desikan, R.S., Segonne, F., Fischl, B., Quinn, B.T., Dickerson, B.C., Blacker, D., Buckner, R.L., Dale, A.M., Maguire, R.P., Hyman, B.T., Albert, M.S., Killiany, R.J., 2006. An automated labeling system for subdividing the human cerebral cortex on MRI scans into gyral based regions of interest. Neuroimage 31, 968–980. doi:10.1016/j.neuroimage.2006.01.021.

Dhollander, T., Connelly, A., 2016. A novel iterative approach to reap the benefits of multi-tissue CSD from just single-shell (+b=0) diffusion MRI data. In: 24th Proceedings of International Society for Magnetic Resonance in Medicine, p. 3010.

Dhollander, T., Mito, R., Connelly, A., 2019a. 3-tissue Compositional Data Analysis of developing HCP (dHCP) diffusion MRI data. In: 25th Annual Meeting of the Organization for Human Brain Mapping, p. 498.

Dhollander, T., Mito, R., Raffelt, D., Connelly, A., 2019b. Improved white matter response function estimation for 3-tissue constrained spherical deconvolution. In: 27th Proceedings of International Society for Magnetic Resonance in Medicine, p. 555.

Dhollander, T., Tabbara, R., Rosnarho-Tornstrand, J., Tournier, J.-D., Raffelt, D., Connelly, A., 2021. Multi-tissue log-domain intensity and inhomogeneity normalisation for quantitative apparent fibre density. In: 29th Proceedings of International Society for Magnetic Resonance in Medicine, p. 2472.

Dibble, M., Ang, J.Z., Mariga, L., Molloy, E.J., Bokde, A.L.W., 2021. Diffusion tensor imaging in very preterm, moderate-late preterm and term-born neonates: a systematic review. J. Pediatr. 232, 48–58. doi:10.1016/j.jpeds.2021.01.008, e43.

Fischl, B., 2012. FreeSurfer. Neuroimage 62, 774–781. doi:10.1016/j.neuroimage.2012.01.021.

Hadaya, L., Nosarti, C., 2020. The neurobiological correlates of cognitive outcomes in adolescence and adulthood following very preterm birth. Semin. Fetal Neonatal Med. 25, 101117. doi:10.1016/j.siny.2020.101117.

Henderson, S.E., Sugden, D.A., Barnett, A.L., 2007. Movement Assessment Battery for Children-2: Movement ABC-2: Examiner's Manual. Pearson, London.

Jenkinson, M., Beckmann, C.F., Behrens, T.E., Woolrich, M.W., Smith, S.M., 2012. Fsl. Neuroimage 62, 782–790. doi:10.1016/j.neuroimage.2011.09.015.

Jones, D.K., Knosche, T.R., Turner, R., 2013. White matter integrity, fiber count, and other fallacies: the do's and don'ts of diffusion MRI. Neuroimage 73, 239–254. doi:10.1016/j.neuroimage.2012.06.081.

Kaufman, A.S., Kaufman, N.L., 1997. Kaufman Brief Intelligence Test, Second Edition (KBIT-2) Manual. NCS Pearson, Minneapolis, MN.

Kelley, M.H., Wu, W.W., Lei, J., McLane, M., Xie, H., Hart, K.D., Pereira, L., Burd, I., Maylie, J., 2017. Functional changes in hippocampal synaptic signaling in offspring survivors of a mouse model of intrauterine inflammation. J Neuroinflammation 14, 180. doi:10.1186/s12974-017-0951-1.

Kellner, E., Dhital, B., Kiselev, V.G., Reisert, M., 2016. Gibbs-ringing artifact removal based on local subvoxel-shifts. Magn. Resonance Med. 76, 1574–1581. doi:10.1002/mrm.26054.

Kelly, C.E., Thompson, D.K., Chen, J., Leemans, A., Adamson, C.L., Inder, T.E., Cheong, J.L., Doyle, L.W., Anderson, P.J., 2016. Axon density and axon orientation dispersion in children born preterm. Hum. Brain Mapp. 37, 3080–3102. doi:10.1002/hbm.23227.

Kelly, C.E., Thompson, D.K., Genc, S., Chen, J., Yang, J.Y., Adamson, C., Beare, R., Seal, M.L., Doyle, L.W., Cheong, J.L., Anderson, P.J., 2020. Long-term development of white matter fibre density and morphology up to 13 years after preterm birth: A fixel-based analysis. Neuroimage 220, 117068. doi:10.1016/j.neuroimage.2020.117068.

Keunen, K., Kersbergen, K.J., Groenendaal, F., Isgum, I., de Vries, L.S., Benders, M.J., 2012. Brain tissue volumes in preterm infants: prematurity, perinatal risk factors and neurodevelopmental outcome: a systematic review. J. Matern. Fetal Neonatal Med. 25 (Suppl 1), 89–100. doi:10.3109/14767058.2012.664343.

Khan, W., Egorova, N., Khlif, M.S., Mito, R., Dhollander, T., Brodtmann, A., 2020. Three-tissue compositional analysis reveals in-vivo microstructural heterogeneity of white matter hyperintensities following stroke. Neuroimage 218, 116869. doi:10.1016/j.neuroimage.2020.116869.

Khan, W., Khlif, M.S., Mito, R., Dhollander, T., Brodtmann, A., 2021. Investigating the microstructural properties of normal-appearing white matter (NAWM) preceding conversion to white matter hyperintensities (WMHs) in stroke survivors. Neuroimage 232, 117839. doi:10.1016/j.neuroimage.2021.117839.

Kidokoro, H., Neil, J.J., Inder, T.E., 2013. New MR imaging assessment tool to define brain abnormalities in very preterm infants at term. AJNR Am. J. Neuroradiol. 34, 2208–2214. doi:10.3174/ajnr.A3521.

Lee, J., Hyun, J.W., Lee, J., Choi, E.J., Shin, H.G., Min, K., Nam, Y., Kim, H.J., Oh, S.H., 2021. So You Want to Image Myelin Using MRI: An Overview and Practical Guide for Myelin Water Imaging. J. Magn. Reson. Imaging 53, 360–373. doi:10.1002/jmri.27059.

Li, K., Sun, Z., Han, Y., Gao, L., Yuan, L., Zeng, D., 2015. Fractional anisotropy alterations in individuals born preterm: a diffusion tensor imaging meta-analysis. Dev. Med. Child Neurol. 57, 328–338. doi:10.1111/dmcn.12618.

Mito, R., Dhollander, T., Xia, Y., Raffelt, D., Salvado, O., Churilov, L., Rowe, C.C., Brodtmann, A., Villemagne, V.L., Connelly, A., 2020. In vivo microstructural heterogeneity of white matter lesions in healthy elderly and Alzheimer's disease participants using tissue compositional analysis of diffusion MRI data. Neuroimage Clin. 28, 102479. doi:10.1016/j.nicl.2020.102479.

Mowinckel, A.M., Vidal-Piñeiro, D., 2019. Visualisation of brain statistics with R-packages ggseg and ggseg3d. ArXiv191208200 Stat. doi:10.1177/2515245920928009.

Newman, B.T., Dhollander, T., Reynier, K.A., Panzer, M.B., Druzgal, T.J., 2020. Test-retest reliability and long-term stability of three-tissue constrained spherical deconvolution methods for analyzing diffusion MRI data. Magn. Reson. Med. 84, 2161–2173. doi:10.1002/mrm.28242.

Nosarti, C., Giouroukou, E., Healy, E., Rifkin, L., Walshe, M., Reichenberg, A., Chitnis, X., Williams, S.C., Murray, R.M., 2008. Grey and white matter distribution in very preterm adolescents mediates neurodevelopmental outcome. Brain 131, 205–217. doi:10.1093/brain/awm282.

Ouyang, M., Dubois, J., Yu, Q., Mukherjee, P., Huang, H., 2019. Delineation of early brain development from fetuses to infants with diffusion MRI and beyond. Neuroimage 185, 836–850. doi:10.1016/j.neuroimage.2018.04.017.

Pandit, A.S., Ball, G., Edwards, A.D., Counsell, S.J., 2013. Diffusion magnetic resonance imaging in preterm brain injury. Neuroradiology 55 (Suppl 2), 65–95. doi:10.1007/s00234-013-1242-x.

Pannek, K., Fripp, J., George, J.M., Fiori, S., Colditz, P.B., Boyd, R.N., Rose, S.E., 2018. Fixel-based analysis reveals alterations is brain microstructure and macrostructure of preterm-born infants at term equivalent age. Neuroimage Clin. 18, 51–59. doi:10.1016/j.nicl.2018.01.003.

Papile, L.A., Burstein, J., Burstein, R., Koffler, H., 1978. Incidence and evolution of subependymal and intraventricular hemorrhage: a study of infants with birth weights less than 1,500 gm. J. Pediatr. 92, 529–534. doi:10.1016/s0022-3476(78)80282-0.

Pecheva, D., Tournier, J.D., Pietsch, M., Christiaens, D., Batalle, D., Alexander, D.C., Hajnal, J.V., Edwards, A.D., Zhang, H., Counsell, S.J., 2019. Fixel-based analysis of the preterm brain: Disentangling bundle-specific white matter microstructural and macrostructural changes in relation to clinical risk factors. Neuroimage Clin. 23, 101820. doi:10.1016/j.nicl.2019.101820.

Raffelt, D., Tournier, J.D., Fripp, J., Crozier, S., Connelly, A., Salvado, O., 2011. Symmetric diffeomorphic registration of fibre orientation distributions. Neuroimage 56, 1171–1180. doi:10.1016/j.neuroimage.2011.02.014.

Saigal, S., Doyle, L.W., 2008. An overview of mortality and sequelae of preterm birth from infancy to adulthood. Lancet 371, 261–269. doi:10.1016/S0140-6736(08)60136-1.

Schilling, K.G., Blaber, J., Huo, Y., Newton, A., Hansen, C., Nath, V., Shafer, A.T., Williams, O., Resnick, S.M., Rogers, B., Anderson, A.W., Landman, B.A., 2019. Synthesized b0 for diffusion distortion correction (Synb0-DisCo). Magn. Reson. Imaging 64, 62–70. doi:10.1016/j.mri.2019.05.008.

Smith, S.M., Nichols, T.E., 2009. Threshold-free cluster enhancement: addressing problems of smoothing, threshold dependence and localisation in cluster inference. Neuroimage 44, 83–98. doi:10.1016/j.neuroimage.2008.03.061.

Smyser, T.A., Smyser, C.D., Rogers, C.E., Gillespie, S.K., Inder, T.E., Neil, J.J., 2016. Cortical Gray and Adjacent White Matter Demonstrate Synchronous Maturation in Very Preterm Infants. Cereb. Cortex 26, 3370–3378. doi:10.1093/cercor/bhv164.

Thompson, D.K., Matthews, L.G., Alexander, B., Lee, K.J., Kelly, C.E., Adamson, C.L., Hunt, R.W., Cheong, J.L.Y., Spencer-Smith, M., Neil, J.J., Seal, M.L., Inder, T.E., Doyle, L.W., Anderson, P.J., 2020. Tracking regional brain growth up to age 13 in children born term and very preterm. Nat. Commun. 11, 696. doi:10.1038/s41467-020-14334-9.

Tournier, J.D., Smith, R., Raffelt, D., Tabbara, R., Dhollander, T., Pietsch, M., Christiaens, D., Jeurissen, B., Yeh, C.-H., Connelly, A., 2019. MRtrix3: A fast, flexible and open software framework for medical image processing and visualisation. Neuroimage 202, 116137. doi:10.1016/j.neuroimage.2019.116137.

Volpe, J.J., 2019. Dysmaturation of Premature Brain: Importance, Cellular Mechanisms, and Potential Interventions. Pediatr. Neurol. 95, 42–66. doi:10.1016/j.pediatrneurol.2019.02.016.

Wasserthal, J., Neher, P., Maier-Hein, K.H., 2018. TractSeg - Fast and accurate white matter tract segmentation. Neuroimage 183, 239–253. doi:10.1016/j.neuroimage.2018.07.070.

Young, J.M., Vandewouw, M.M., Mossad, S.I., Morgan, B.R., Lee, W., Smith, M.L., Sled, J.G., Taylor, M.J., 2019. White matter microstructural differences identified using multi-shell diffusion imaging in six-year-old children born very preterm. Neuroimage Clin. 23, 101855. doi:10.1016/j.nicl.2019.101855.

Zhang, Y., Inder, T.E., Neil, J.J., Dierker, D.L., Alexopoulos, D., Anderson, P.J., Van Essen, D.C., 2015. Cortical structural abnormalities in very preterm children at 7 years of age. Neuroimage 109, 469–479. doi:10.1016/j.neuroimage.2015.01.005.

Zhou, L., Zhao, Y., Liu, X., Kuang, W., Zhu, H., Dai, J., He, M., Lui, S., Kemp, G.J., Gong, Q., 2018. Brain gray and white matter abnormalities in preterm-born adolescents: A meta-analysis of voxel-based morphometry studies. PLoS One 13, e0203498. doi:10.1371/journal.pone.0203498.